REPÜLÉSTUDOMÁNYI KÖZLEMÉNYEK
On-Line tudományos folyóirat
XXVII. évfolyam 2015. 2. szám

Foroozan Zare[1] – Árpád Veress[2]

PLAUSIBILITY CHECK OF THE INVERSE DESIGN AND OPTIMIZATION METHOD FOR CASCADE FLOW BY MEANS OF ANSYS CFX SOFTWARE[3][4]

The goal of the present numerical investigation is to verify the correct and plausible operation of the DASFLOW inverse design based in-house optimization tool for cascade flow by the application of ANSYS CFX. Compressible Euler equations are considered in the academic code and a finite volume method has been implemented to solve the governing equations numerically. NACA 65-410 profile has been adopted for constructing a 2D cascade and for providing initial geometry. Stratford's separation prediction method with constrained Sequential Quadratic Programming has been used to determine the optimum pressure distribution at given boundary conditions along the suction side. The optimum pressure distribution is imposed in the inverse design mode of the DASFLOW for evolution of the corresponding contour belongs to that required pressure distribution. Following the determination of the expected profile with the flow field, the results are compared with the outcomes of the ANSYS CFX in inviscid and viscous mode also at the same geometry, mesh, boundary conditions, material properties and physical settings.

INVERZ TERVEZŐ ÉS OPTIMALIZÁCIÓS MÓDSZER PLAUZIBILITÁS-VIZSGÁLATA LAPÁTRÁCSBAN KIALAKULT ÁRAMLÁS ESETÉN ANSYS CFX SZOFTVER SEGÍTSÉGÉVEL

A jelen kutatási jelentésben bemutatott numerikus áramlástani vizsgálat célja, hogy igazolja a tanszéki fejlesztésű DASFLOW inverz tervező és optimalizációs eszköz működésének helyességét és az eredmények hitelességét ANSYS CFX szoftver segítségével. Az akadémiai program alapegyenletei az összenyomható közegre felírt Euler egyenletek, amelyek numerikus megoldását cella központú véges térfogat módszerével végeztük el. A vizsgálat tárgyát képező 2D-s lapátrács elkészítéséhez a NACA 65-410 profilt használtuk fel. A profil körül kialakuló optimális szívott oldali nyomáseloszlás meghatározásának érdekében Stratford leválás előrejelző módszerét implementáltuk a korlátos szekvenciális kvadratikus programozás folyamatába. Az optimális nyomáseloszlás előírását követően a DASFLOW program inverz tervező modulja előállította az optimális nyomáseloszláshoz tartozó profilt. Az eredményeket ANSYS CFX program által - azonos geometriai modell, háló, peremfeltételek, anyag-, és fizikai tulajdonságok beállítása mellett, súrlódásos és súrlódásmentes esetben - előállított eredményekkel hasonlítottuk össze.

[1] Foroozan Zare, PhD student, BME, Department of Aeronautics, Naval Architecture and Railway Vehicles, fzare@vrht.bme.hu

[2] Dr. Árpád Veress, associate professor, BME, Department of Aeronautics, Naval Architecture and Railway Vehicles, averess@vrht.bme.hu

[3] Reviewed: Prof. Dr. László Pokorádi, professor, Óbudai University, pokoradi.laszlo@bgk.uni-obuda.hu

[4] Reviewed: Prof. Dr. Szabolcsi Róbert, professor, Óbudai University, szabolcsi.robert@bgk.uni-obuda.hu

NOMENCLATURE

Variables (Latin)

c	[m, m/s]	chord length, sound speed
C_p	[-,$J/kg/K$]	pressure coefficient, spec. heat
D	[-]	Jacobian matrix
E	[J/kg]	mass specific total energy
F, G	[-]	inviscid flux vectors
h_0	[J/kg,-]	mass specific total enthalpy
H	[var.]	vector of num. flux function
n_x, n_y	[m]	components of normal vector
p	[Pa]	static pressure
R	[$J/kg/K$]	spec. gas const., residual [var.]
s	[s,-]	unit normal direction to n
t	[s]	time
U	[-]	vector of conservative var.
u,v	[m/s]	components of velocity vector
V_n	[m/s]	velocity normal to the surface
W	[-]	vector of characteristic var.
x, y	[m]	Cartesian coordinates in space

Variables (Greek)

α	[deg,-]	inlet flow angle, angle of attack
α_k	[-]	const. for the Runge-Kutta time iteration
γ	[-]	ratio of specific heats
Γ	[m]	cell face length
Δ	[-]	difference
$\lambda_n^{(i)}$	[m/s]	normal eigenvalues
ρ	[kg/m^3]	density
χ	[-]	Roe's average density
Ω	[m^2]	area of the finite volume

Subscripts and Superscripts

$\bar{}$	vector
~	Flux function
ˆ	Roe's average state space
0	total parameters (pressure, temperature)
1	upstream condition
i,j,k	variables for spatial and sum indexing
in, out	inlet and outlet
l	local variable (static pressure)
n	variables normal to the surface
$n+1$	param. at the boundary (next time step)
req	required
$stat$,to	static, total

Abbreviations

BC	:	Boundary Condition
CFD	:	Computational Fluid Dynamics
CFL	:	Courant number
L	:	Left side of the cell interface
Le	:	leading edge
MUSCL:		Monotone Upstream Schemes for Conservation Laws
NBC	:	Numerical Boundary Condition
PBC	:	Physical Boundary Condition
R	:	Right side of the cell interface
Re	:	Reynolds number
RK	:	Runge-Kutta
SQP	:	Sequential Quadrat. Programming
Te	:	Trailing edge
var.	:	variable

INTRODUCTION

In the last decade, the advantages of the Computational Fluid Dynamics (CFD) have been utilized in the research and design processes more than ever before not only in industrial level, but in the academic one also. Many ongoing activities are available in that field ([19], [20] and [21]). Applying CFD techniques, the numerous experiments can be replaced, by which significant amount of cost, capacity and time can be saved. Parameterization provides higher reproducibility and flexibility in the model generation and it allows calculation processes with higher level automation. The wide range of the visualisation tools get insight into the origin of the problem much deeper as it was ever before. Although the consistency, stability and convergence characteristics of the different numerical methods have been investigated and proved, the

plausibility check, as verification or validation for example must be completed to be convinced about the correctness and the accuracy. The most suitable approach amongst them is the validation, in which the simulation results are compared with the measured ones. The other benchmarking could be to compare the outputs of the newly developed CFD software with the results of existing, well established, reliable, verified and validated tools as commercial programs for instance. Here, in the present research, the main goal is to verify the correct and plausible operation of the DASFLOW inverse design based in-house optimization tool for cascade flow by the application of a commercial CFD software: ANSYS CFX.

If the verification and the validation over the expected and reasonable wide range of the fluid dynamics problem proves the applicability of the method – according to which, in general, the differences between the measured and simulated results are less than 5% – the available technique allows the universities, institutes and companies to turn more effort on the these fields of the engineering activity; recently called virtual prototyping, which is one of the most beneficial and rapidly developing technologies nowadays. Additionally, in case of applying optimization methods with CFD, not only the development process, but the overall efficiency of the new products can also be increased significantly.

Optimization Methods and Their Ability to be Coupled with CFD

Beside the developments of the central core of the fluid dynamics solvers, the different optimization techniques, coupled with CFD, are also under intensive research [15]. In case of direct optimization techniques, an attempt has been made to find the optimal solution. They typically utilize some sort of search technique (gradient-based optimizer), stochastic based algorithms (e.g. evolutionary strategies, genetic algorithms) and artificial neural networks for example. These procedures can be computationally expensive because several flow solutions must be completed to specify for example the direction of deepest descent, fitness of individuals in the population in order to determine the shape changes. Furthermore, the required number of flow solutions increases dramatically with the number of design variables.

Several optimization methods have been developed so far, but the optimal shapes for practical CFD design have been the subject of limited methods.

Inverse Design Based Optimization

In case the inverse design-type methods, the geometry modification is based on the prescribed set of the pre-defined variables at the wall by simple, fast and robust algorithms, which makes them especially attractive amongst other optimization techniques. The wall modification can be completed within much less flow solutions for inverse design techniques than for direct optimization methods. Hence, the inverse design methods typically being much more computationally efficient and they are very innovative to be used in practice. The main drawback of the inverse design methods is that the designer should create target (optimum in a specific sense) pressure or velocity distributions that should correspond to the design goals and meet the required

aerodynamic characteristics. However, it can be difficult to specify the required pressure or velocity distribution that satisfies all the design goals. Also, one cannot guarantee that an arbitrarily prescribed pressure/velocity distribution will provide mechanically correct airfoils without trailing edge open or cross over [17].

Without high performance computing, the earliest methods of inverse design were analytical. Jacobs, Theodorsen, Mangler and Lighthill [9] can be considered as pioneer in this field by developing an inverse design method for 2D incompressible flow past airfoils, making use of conformal mapping and potential flow solution. These methods are limited to the shock-free irrotational flows and difficult to extend to 3D. At the last decades of the twenty century, the inverse methods are rather based on an iterative solution and they are generally developed together with the newly developed CFD solvers mostly based on the theory of characteristics. The governing equations of those methods are generally the Euler and Navier-Stokes equations. The solid wall modification algorithm is performed by means of transpiration technique (Giles and Drela [4], Demeulenaere [2] and De Vito [3]). These methods are primarily dedicated to the design of airfoils, wings and turbomachinery cascades, but it has also been applied for design of duct geometries (Cabuk and Modi [1]) [17].

The general procedure of the iterative type inverse design methods requires an initial geometry and optimal pressure or velocity distribution over the wall to be modified. The prescribed distribution is generally comes from the industrial experiences and/or theory. The iterative cycle starts with the direct solution of a CFD solver. Completing the convergence criteria, a new boundary condition is applied at the solid boundary to be optimized, by which the wall become locally opening as inlet or outlet, depends upon the evolved pressure distribution between the boundary and computational domain. The outcome of this analysis is a velocity distribution along the wall, which is not necessarily parallel with it. The final step of the cycle is the wall modification. The wall becomes parallel with the local velocity vector corresponds to a new streamline of the flow field. The mentioned procedure is repeated until the target distribution is reached by the direct analysis and so the new geometry is available [17].

Two dimensional inviscid inverse design based optimization method has been introduced, tested and verified by using ANSYS CFX commercial software in the present report. First, the numerical method is described in the second chapter to be used in the DASFLOW academic code. It has been followed by the introduction of the constraint optimization method coupled with Stratford's separation prediction theory in chapter three. NACA 65-410 profile has been used to construct the cascade to have initial flow field for the inverse design method. The description of the design by means of profile contour evolution to fit for the optimum and so the expected pressure distribution is found in chapter 4. The available results of the in-house code are then compared with the results the ANSYS CFX commercial software in inviscid and viscous manner at the same geometry, mesh, boundary conditions, material properties and physical settings. The comparison and the outcomes of the agreement between the two approaches are presented in chapter 5.

Governing Equations

Due to the aeronautical application with the assumption of no separation, the conservative form of the unsteady 2D compressible Euler equations has been used as a governing equations for rotational flow modelling, which are given in Cartesian coordinate system by (1) [10] in Λ(x,y),

$$\frac{\partial U}{\partial t}+\frac{\partial F(U)}{\partial x}+\frac{\partial G(U)}{\partial y}=0, \tag{1}$$

where $x, y \in \mathbf{R}$ and $t \in \mathbf{R}^{+}$. The conservative variables and convective fluxes are given by (2),

$$U=\begin{pmatrix}\rho\\ \rho u\\ \rho v\\ \rho E\end{pmatrix},\ F(U)=\begin{pmatrix}\rho u\\ \rho u^2+p\\ \rho uv\\ \rho u h_0\end{pmatrix},\ G(U)=\begin{pmatrix}\rho v\\ \rho vu\\ \rho v^2+p\\ \rho v h_0\end{pmatrix}, \tag{2}$$

where ρ is the density, u and v are the Cartesian components of velocity and p is the static pressure. The specific total energy and enthalpy is the following:

$$E=\frac{1}{\gamma-1}\frac{p}{\rho}+\frac{u^2+v^2}{2},\ h_0=\frac{\gamma}{\gamma-1}\frac{p}{\rho}+\frac{u^2+v^2}{2}. \tag{3}$$

The γ is the ratio of specific heats.

Finite Volume Discretization Method

Integrating system eq. (1) over a control surface Ω, which is bounded by interface Γ, and applying the Gauss divergence theorem gives [10]:

$$\frac{\partial}{\partial t}\iint_{\Omega} U d\Omega+\int_{\Gamma}\vec{H}\vec{n}d\Gamma=0, \tag{4}$$

where $\vec{n}=(n_x,n_y)$ is the local outward pointing unit normal vector of the cell boundary, $\vec{H}=F\vec{e}_x+G\vec{e}_y$ and $\vec{H}\vec{n}$ is given by

$$H_n=\vec{H}\vec{n}=\begin{pmatrix}\rho V_n\\ \rho u V_n+pn_x\\ \rho v V_n+pn_y\\ \rho V_n h_0\end{pmatrix}, \tag{5}$$

where

$$V_n=\vec{V}\vec{n}=(u\vec{e}_x+v\vec{e}_y)(n_x\vec{e}_x+n_y\vec{e}_y). \tag{6}$$

Finite volume method has been applied for the discretization. The second integral in eq. (4) is replaced by summation over the all boundaries N_b of the control surface Ω_j. Eq. (4) can be written in the following semi-discrete form for the point, j:

$$\frac{d}{dt}U_j = -\frac{1}{\Omega_j}\sum_{k=1}^{N_b}\left[H_n\right]_{j,k}\Gamma_{j,k} = \Re_j, \tag{7}$$

where $\left[H_n\right]_{j,k}$ is the total inviscid flux normal to the cell boundary at cell face boundary k and U_j is the vector of conservative variables (2). In present case, in 2D, Ω_j is the area of the finite surface and $\Gamma_{j,k}$ is the length of a cell boundary number k of Ω_j. In case of upstream differencing (or upwind) schemes, the quantity $\left[H_n\right]_{j,k}$ are characterized by a flux function $\hat{H}_n$, which takes into account the sign of the Jacobian matrices, or in other words the relevant propagation directions between the left (L) and right (R) states (sides) of the cell boundary [10],

$$\hat{H}_n\left(U^L, U^R\right). \tag{8}$$

The $\hat{H}_n\left(U^L, U^R\right)$ can be evaluated by linear wave decomposition where an unique average state (which is denoted by a hat) of the left and right states exist [11]:

$$\hat{H}_n\left(U^L, U^R\right) = \frac{1}{2}\left\{H_n\left(U^L\right) + H_n\left(U^R\right) - \left|\hat{D}_n\left(U^L, U^R\right)\right|\left(U^R - U^L\right)\right\}. \tag{9}$$

For the ideal gas, Roe has shown that the matrix $\hat{D}_n$ is equal to the Jacobian D_n [11] when expressed as a function of the variables of $\hat{\rho}$, $\hat{u}$, $\hat{v}$, and $\hat{h}_0$, which are weighted variables of the square root of density. Detailed information about the Roe's method of the approximate Riemann solver is found in [11]. The method of Roe is highly non-dissipative and closely linked to the concept of characteristic transport. It is one of the most powerful linear Riemann solvers due to the excellent discontinuity-capturing property including shear waves. However, it is well-known that flux function mentioned above can produce non-physical expansion shocks that violate the entropy condition. This can be avoided, by modifying the modulus of the eigenvalues for the non-linear fields and method of Yee [16] is used at the present case.

MUSCL (Monotone Upstream Schemes for Conservation Laws) approach is implemented for higher order spatial extension by which, the piece-wise constant distribution of the initial variables over the cell can be replaced by a piecewise linear or quadratic one. The mathematical deduction starts with the introduction of Taylor series expansion around point i:

$$U(x) = U_i + \frac{\partial U}{\partial x}\Big|_{x_i}\left(x - x_i\right) + \frac{1}{2}\frac{\partial^2 U}{\partial x^2}\Big|_{x_i}\left(x - x_i\right)^2 + O\left(\Delta x^3\right). \tag{10}$$

The x spatial direction corresponds to local curvilinear coordinate in each direction. After discretization and integration (10) yields:

$$\left(U^R = \right)\overline{U}^R_{i+\frac{1}{2}} = U_{i+1} - \frac{1}{4}\left[\left(1-\kappa\right)\Delta_{i+\frac{3}{2}} + \left(1+\kappa\right)\Delta_{i+\frac{1}{2}}\right],$$

$$\text{and } \left(U^L = \right)\overline{U}^L_{i+\frac{1}{2}} = U_i + \frac{1}{4}\left[\left(1-\kappa\right)\Delta_{i-\frac{1}{2}} + \left(1+\kappa\right)\Delta_{i+\frac{1}{2}}\right] \tag{11}$$

where $\Delta_{i-\frac{1}{2}} = U_i - U_{i-1}$, $\Delta_{i+\frac{1}{2}} = U_{i+1} - U_i$, $\Delta_{i+\frac{3}{2}} = U_{i+2} - U_{i+1}$ and the new left and right states next to the cell boundary $i+\frac{1}{2}$ (between points *i* and *i+1*) are denoted by U^L, and U^R. The $\kappa = 1/3$ in equation (11) corresponds to the third order accurate space discretization in one dimensional problem [10]. The spurious oscillations (wiggles) can occur with high order spatial discretization schemes due to shocks, discontinuities or sharp changes in the solution domain. Hence, in this case, Mulder limiter is implemented in the high resolution schemes for monotonicity preserving [10]:

$$\left(U^R = \right)\overline{U}^R_{i+\frac{1}{2}} = U_{i+1} - \frac{1}{4}\psi^R\left[\left(1-\kappa\psi^R\right)\Delta_{i+\frac{3}{2}} + \left(1+\kappa\psi^R\right)\Delta_{i+\frac{1}{2}}\right], \tag{12}$$

$$\left(U^L = \right)\overline{U}^L_{i+\frac{1}{2}} = U_i + \frac{1}{4}\psi^L\left[\left(1-\kappa\psi^L\right)\Delta_{i-\frac{1}{2}} + \left(1+\kappa\psi^L\right)\Delta_{i+\frac{1}{2}}\right], \tag{13}$$

where

$$\psi^R = \frac{2\Delta_{i+\frac{1}{2}}\Delta_{i+\frac{3}{2}} + \varepsilon}{\Delta^2_{i+\frac{1}{2}} + \Delta^2_{i+\frac{3}{2}} + \varepsilon}, \quad \psi^L = \frac{2\Delta_{i-\frac{1}{2}}\Delta_{i+\frac{1}{2}} + \varepsilon}{\Delta^2_{i-\frac{1}{2}} + \Delta^2_{i+\frac{1}{2}} + \varepsilon}, \quad 10^{-7} \le \varepsilon \le 10^{-5} \tag{14}$$

A widely used class of non-linear multi-stage time integration techniques is given by the Runge-Kutta (RK) schemes. They are usually designed to obtain higher order temporal accuracy with minimum computational storage and the large stability range with the specific coefficients, even though it has been often used for steady state calculations as herein. The 4 stages RK method (RK4) is used to solve the time derivatives of the conservative variables (7) [10]:

$$\begin{aligned} U^0 &= U^n \\ U^k &= U^0 + \alpha_k \Delta t \Re\left(U^{k-1}\right), \quad k = 1,...,4, \\ U^{n+1} &= U^m \end{aligned} \tag{15}$$

where $\alpha_1 = \frac{1}{8}$, $\alpha_2 = 0.306$, $\alpha_3 = 0.587$, $\alpha_4 = 1$ [5], *n* is the previous time step and *n+1* is the next time step. The RK4 index is denoted by *k* and it runs from 1 to *m* with its maximum value of 4. Due to the steady state assumption, the time accuracy is not required; hence the RK4 coefficients are applied to have high stability and smoothing properties of the upwind scheme with MUSCL reconstruction. In order to optimize the time step behind the stability criterion, the local time stepping has been used for every cells j as follows [8]:

$$\Delta t_j = \frac{\Omega_j \nu}{\sum_{k=1}^{N_b} \left(|V_n| + c\right)_{j,k} \Gamma_{j,k}}, \tag{16}$$

where Ω_j is the area of the finite surface j, ν is the Courant number, $\Gamma_{j,k}$ is the length of the cell boundary k of Ω_j, V_n is the cell face normal velocity and c is the sound speed. Detailed description of the finite volume discretization and the analysis of numerical methods are found in [7] and [13].

Boundary Conditions

The numerical treatment of the boundary conditions strongly influences not only the convergence properties but the accuracy of the results in solving partial differential equations. The hyperbolic system that consists of Ne partial differential equations, Np ≤ Ne physical boundary conditions (PBC) and Nn = Ne − Np numerical boundary conditions (NBC) necessary to be prescribed [6]. The former must secure the existence and uniqueness of the exact solution, while the latter are supposed to ensure that various perturbations generated in the interior of the computational domain leave it without being reflected at the boundaries [5]. Hence, a proper combination of PBC and NBC must be imposed by means of some extra calculations.

The characteristic form of the governing equations in outward cell face normal direction yields a sequence of decoupled convection equations as follows [7]:

$$\begin{aligned}
&\frac{\partial W_n^{(1)}}{\partial t} + V_n \frac{\partial W_n^{(1)}}{\partial n} = 0; \\
&\frac{\partial W_n^{(2)}}{\partial t} + V_n \frac{\partial W_n^{(2)}}{\partial n} = 0; \\
&\frac{\partial W_n^{(3)}}{\partial t} + \left(V_n + c\right)\frac{\partial W_n^{(3)}}{\partial n} = 0; \\
&\frac{\partial W_n^{(4)}}{\partial t} + \left(V_n - c\right)\frac{\partial W_n^{(4)}}{\partial n} = 0;
\end{aligned} \tag{17}$$

Where n is the unit normal direction to the cell face, V_n is the scalar product of vector $\vec{V}$ and n, c is the sound speed and W_n is the characteristic variables or Riemann invariants. These invariants are transported along the characteristic curves at the respective speeds. The direction of wave propagation (V_n, V_n, V_n+c, V_n-c) depends not only on the sign of the velocity V_n but also on the local speed of sound c. At the boundary, the number of PBC to be imposed equals the number of negative eigenvalues, which correspond to the incoming characteristics from the outside (boundary) to the computational domain. The need for NBCs comes from the fact that the actual problem to be solved is formulated in terms of the conservative variables rather than Riemann invariants. Therefore, it is impossible to impose the Dirichlet boundary conditions in the usual way. It is common practice to recover the boundary values by changing to the characteristic

variables, evaluating the incoming Riemann invariants from the PBCs and extrapolating the outgoing ones from the interior of the computational domain [6].

Regarding the specific and detailed description of the inlet, outlet, solid wall, opening and periodic boundary conditions in theoretical manner, they are found in [17].

Wall Modification Algorithm

While the incoming and out coming velocity distribution is given at the solid wall, based on the inverse mode of the analysis by using so called opening boundary condition, the last step of the iterative design cycle is the modification of the geometry. The new position of the solid boundary coordinates are calculated by setting the wall parallel to the local velocity vector:

$$\Delta y_i(x_i) = \sum_{k=Le}^{i} \left(\frac{v_k}{u_k} \Delta x_k \right), \tag{18}$$

where u and v are the Cartesian component of the velocity vector. The wall modification starts from the leading edge or inlet stagnation point till the trailing edge or the outlet stagnation point and completed in vertical directions (see Fig. 1.).

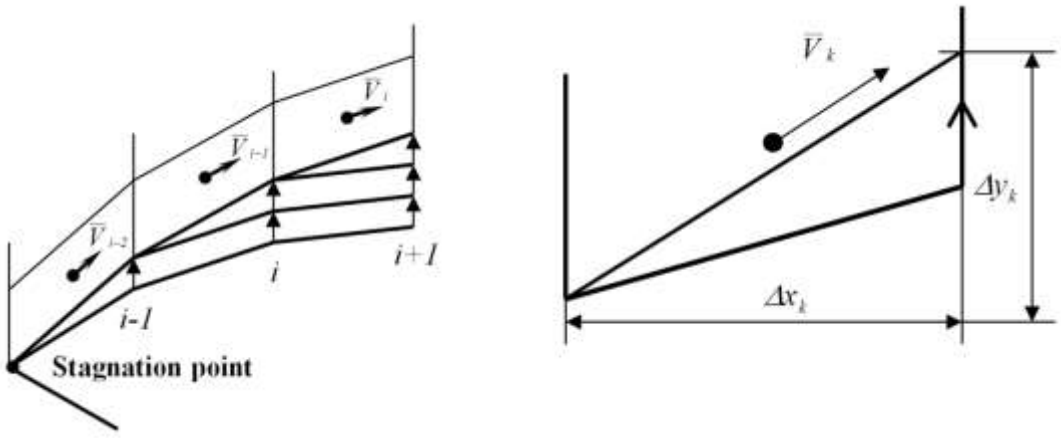

Figure 1 Schematic view of the wall modification process based on the local velocity vector [17]

Constraint OptimiZation [17]

The inverse design methods require optimal pressure or velocity distributions to determine the adherent geometry. Hence, the main goal of the present chapter is to introduce the complete procedure how the pressure distribution is optimized. The method is based on Stratford's experimental investigation on separation prediction and SQP (Sequential Quadratic Programming) nonlinear constraint optimization algorithm.

Stratford's Separation Prediction Method

In order to maximise the blade loading or the lift force of the suction side of a profile at given and constant operational (boundary) conditions, the pressure distribution should be as low as possible over the solid surface. However, the adverse pressure gradient must be present after the location of the maximum velocity (and minimum pressure) in order to recover downstream conditions. The adverse pressure gradient till the trailing edge should have limited in each discretized points to be just below the condition of causing separation. The maximum area bounded by the suction and the pressure side distributions in conjunction with the mentioned limited values of pressure gradients will provide the optimum solution as a target distribution to be specified for the inverse design method.

There are several existing methods for predicting separation as Goldschmied, Stratford, Head, and Cebeci-Smith for example. The accuracy these methods were examined several times. One of the output of these investigation shows that the operation of Goldschmied's method is unreliable. The other three are in reasonable agreement and Stratford's method tended to predict separation slightly early. The Cebeci-Smith method is appeared to be the best and the Head method is a strong second one [12]. Due to the good accuracy, simple expressions and conservative characteristics for predicting separation, Stratford's method has been used in followings.

Stratford has derived an empirical formula for predicting the point of separation in an arbitrary decelerating flow at the order of Re=10E6 [14],

$$\frac{\overline{C}_p\left[x\left(d\overline{C}_p/dx\right)\right]^{1/2}}{\left(10^{-6}\,\mathrm{Re}\right)^{1/10}} = S\,, \tag{19}$$

where the canonical pressure distribution is

$$\overline{C}_p = \frac{p - p_0}{\frac{1}{2}\rho_0 u_0^2} \tag{20}$$

and if $d^2p/dx^2 \geq 0$ then S = 0.39 or if $d^2p/dx^2 < 0$ then S =0.35. Additionally, $\overline{C}_p \leq 4/7$. The flows under investigations consist first of a flat-plate flow. Hence, x is distance measured from the leading edge of the plate, and, $Re = u_0 x/\nu$. If the flows begin the pressure rise at a point x_0 (it is the position of minimum pressure and maximum velocity and its parameters belong to subscript of $_0$), left-hand side of eq. (19) starts from a zero value. The left-hand side then grows. When it reaches the limiting value of S, separation is said to occur. If S is held at its limiting value of 0.39 for $d^2p/dx^2 > 0$ eq. (19) amounts to an ordinary differential equation for $\overline{C}_p(x)$. It is evident from eq. (19) that the equation describes a flow that is ready everywhere to separate. Stratford presents the following solutions [14],

$$\overline{C}_p = 0.645\left\{0.435\,\mathrm{Re}_0^{1/5}\left[\left(x/x_0\right)^{1/5} - 1\right]\right\}^{2/n} \quad for \quad \overline{C}_p \leq (n-2)/(n+1) \tag{21}$$

$$\overline{C}_p = 1 - \frac{a}{\left[\left(x/x_0\right)+b\right]^{1/2}} \quad for \quad \overline{C}_p \geq (n-2)/(n+1). \tag{22}$$

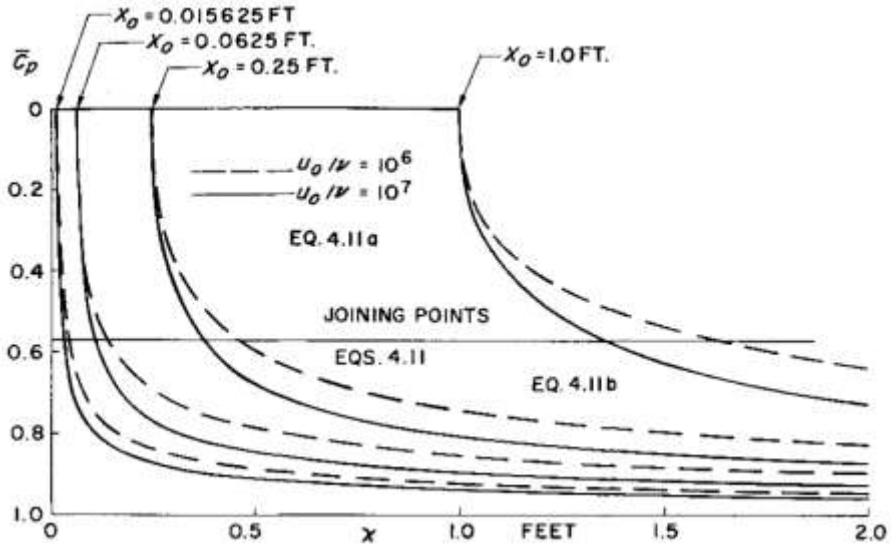

Figure 2 Stratford limiting flows at two values of unit Reynolds number [12]

In that two-part solution (see Fig. 2 also), x_0 is the start of pressure rise, $\mathrm{Re}_0 = u_0 x_0/\nu$, x is the distance measured from the very start of the flow, which begins as flat-plate, turbulent flow. The number n is a constant that Stratford finds to be about 6. The quantities a and b are arbitrary constants used in matching values and slopes in the two equations at the joining point, $\overline{C}_p \geq (n-2)/(n+1)$. Of course, eq. (21) describes the beginning of the flow and eq. (22) the final part. The flow is an equilibrium flow that always has the same margin, if any, against separation.

Constraint Optimization of Stratford's Limiting Pressure Distribution

The method presented above is used for determining the pressure distribution at maximum lift (or blade) force and at the limit of separation on the suction side for given far inlet conditions:

$$\Re\left(\overline{C}_p(x)\right) = \Im\left(C_p(x)\right) = \oint C_p(x)dx = \oint \frac{p - p_\infty}{\frac{1}{2}\rho_\infty u_\infty^2} dx = \oint \frac{p - p_\infty}{0.5\gamma p_\infty M_\infty^2} dx, \tag{23}$$

where p is the static pressure at the given location and the other primitive variables correspond to inlet condition denoted by ∞. The connection between $\overline{C}_p(x)$ and $C_p(x)$ is given by:

$$\overline{C}_p = \frac{p - p_0}{\frac{1}{2}\rho_0 u_0^2} = \frac{C_p - C_{p,0}}{1 - C_{p,0}} = \frac{\frac{p - p_\infty}{\frac{1}{2}\rho_\infty u_\infty^2} - \frac{p_0 - p_\infty}{\frac{1}{2}\rho_\infty u_\infty^2}}{1 - \frac{p_0 - p_\infty}{\frac{1}{2}\rho_\infty u_\infty^2}} = \frac{p - p_0}{p^{total} - p_0} = \frac{p - p_0}{\frac{1}{2}\rho_0 u_0^2}. \quad (24)$$

The objective function is to

$$\text{minimize } \frac{1}{\aleph\left(\overline{C}_p(x)\right)} \quad (25)$$

$$\text{subject to } p_{opt}^{TE} - p_{outlet} = 0. \quad (26)$$

The reason of the constraint to be specified at the presented way is to fix trailing edge condition of Stratford's method expecting that the pressure at the cascade outlet is close to the outlet static pressure.

The optimisation procedure is divided by two sub steps. In the first sub step the physical connections between different parameters are described by Stratford's criteria to evaluate limiting pressure distribution. The pressure coefficient at the minimum pressure (p_0) is given by:

$$C_{p,0} = \frac{p_0 - p_\infty}{\frac{1}{2}\rho_\infty u_\infty^2} = \frac{p_0 - p_\infty}{0.5\gamma p_\infty M_\infty^2} = \frac{p_0 - p_\infty}{0.7 p_\infty M_\infty^2}, \quad (27)$$

where p_0 and maximum velocity u_0 is supposed to be constant starting from the leading edge of the suction side till the starting of the increasing pressure gradient (x_0). The Mach numbers M_0 at these points are calculated by:

$$C_{p,0} = \frac{p_0 - p_\infty}{0.7 p_\infty M_\infty^2} = \frac{1}{0.7 M_\infty^2}\left[\left(\frac{1 + 0.2M_\infty^2}{1 + 0.2M_0^2}\right)^{\frac{\gamma}{\gamma-1}} - 1\right]. \quad (28)$$

The T_0 , u_0 and ρ_0 are given by the energy equation of the isentropic flow and ideal gas law:

$$T_0 = T^{total}\left(1 + \frac{\gamma - 1}{2} M_0^2\right)^{-1}, \quad (29)$$

$$u_0 = \sqrt{\frac{\gamma}{\gamma - 1} R\left(T^{total} - T_0\right)2}, \quad (30)$$

$$\rho_0 = \frac{p_0}{R T_0}. \quad (31)$$

The *total* quantities correspond to the given inlet boundary conditions.

A general way of determining pressure distribution starts with specifying a possible p_0. All parameter belongs to p_0 can be calculated by equations of (27)-(31). The next step is to find location x_0, which gives back the required trailing edge static pressure by using Stratford equations (21) and (22) over *x*. Hence, the location of starting flow deceleration (x_0) and the Stratford's limiting pressure distribution till the required trailing edge pressure is the output of the first sub step of the optimisation procedure. There are infinite possible pressure distribution existing by the presented method and some of them are shown in Fig. 3 at given total quantities for a wing profile NACA 65-410 (only for example).

The second sub step of the optimization procedure is the constraint optimization in order to determine the corresponding flow parameters and location belongs to the minimum pressure and maximum velocity point on the suction surface, which provide the maximum area bounded by the pressure distribution of the suction side of the profile. p_0, T_0, u_0, ρ_0, x_0 and $p(x)$ (by Stratford's criteria) parameters will be modified in the second sub step to satisfy (25).

The pressure side distribution is also modified in order to keep the trailing edge closed. Linear distribution has been used (see Fig. 8.) with keeping open further investigations in the direction of less choking and drag (axial force) reduction.

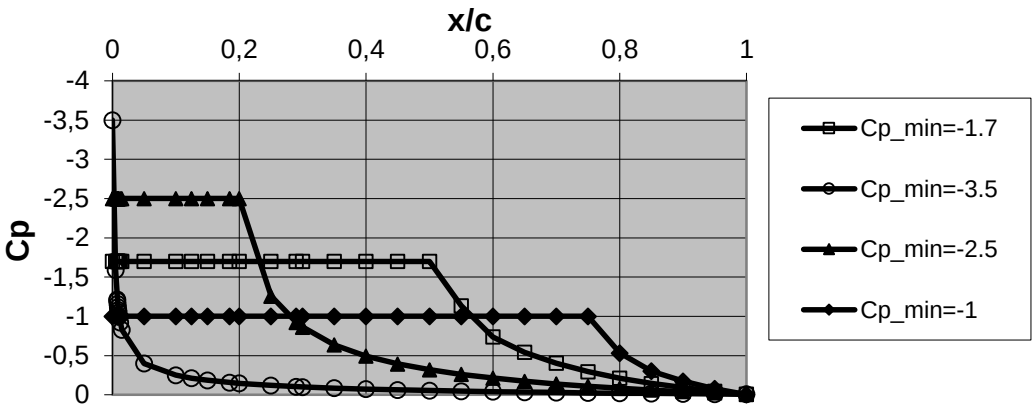

Figure 3 Suction side pressure distribution using Stratford pressure distribution close to the separation ($C_p \approx 0$ at trailing edge) for wing profile NACA 65-410 (only for example, different curve is used in the next chapter)

The flowchart of the whole optimization process coupled with the inverse design method is found in Fig. 4.

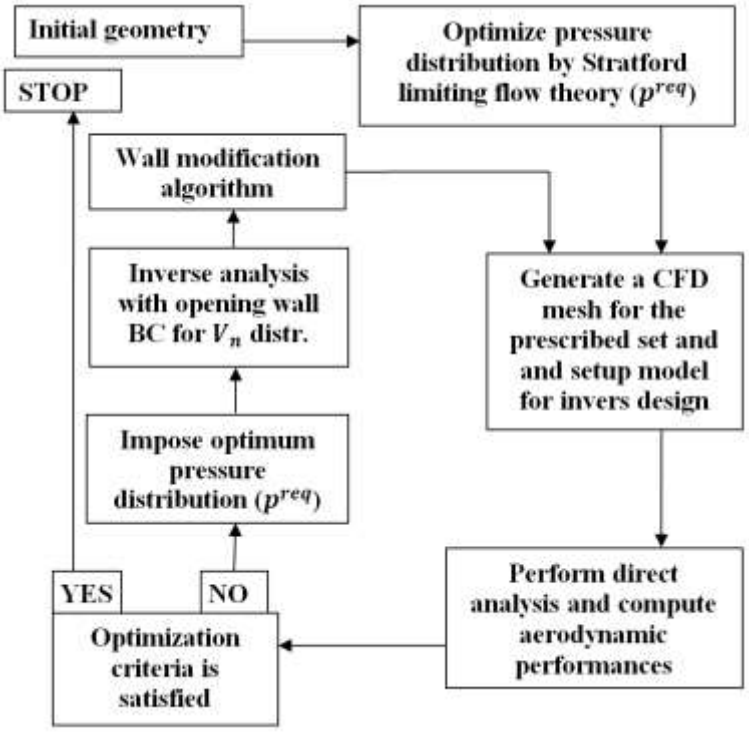

Figure 4 Flowchart of the optimization process

NUMERICAL TESTING OF THE INVERSE DESIGN METHOD ON THE NACA 65-410 CASCADE FLOW

The goal of the present chapter is to complete numerical investigations in order to verify the correct operation of the inverse design based optimization procedure described before and summarizing here.

The used iterative inverse design method requires an initial geometry and optimal (in specific sense) pressure distribution over the wall to be modified. The optimal pressure distribution is generated by SQP nonlinear constraint optimisation with the goal function of maximising profile loading with respect to inlet and outlet conditions. Additionally, the pressure distribution is restricted to follow Stratford's separation prediction method to be close but safe distance far from the separation in the decelerating flow conditions. The iterative cycle starts with the direct solution of a CFD solver. After completing the convergence criteria, a new boundary condition is applied at the solid boundary to be optimized, by which the wall become locally opening as inlet or outlet, depends upon the evolved pressure distribution between the boundary and computational domain. The outcome of this analysis is a velocity distribution along the wall, which is not necessarily parallel with it. The final step of the cycle is the wall modification. The wall becomes parallel with the local velocity vector corresponds to a new streamline of the flow field. The mentioned procedure is repeated until the target distribution is reached by the direct analysis and so the new geometry is available [17].

NACA 65-410 profile has been used for preparing the initial geometry. The chord angle measured to the axial direction is 30° and the angle of attack is 0°. The boundary conditions are specified to be in the corresponding range of Re, which is valid for Stratford flow limiting theory (at the order of Re=10E6) and they are the followings: inlet total pressure: $p_{tot,in}$=107853.4 [Pa]; inlet total temperature: $T_{tot,in}$=298.4 [K]; outlet static pressure: $p_{stat,out}$=101325 [Pa] over the H-type mesh (110×60). The resulted flow field for the initial geometry is found in subchapter 4.1 and the application of the inverse design method based optimization procedure with the resulted geometry and flow field are presented in subchapter 4.2 respectively.

Numerical Analysis of Initial Geometry

The Mach number, static pressure and static temperature distributions are plotted in Fig. 5-7. The results are acceptable in the physical point of view.

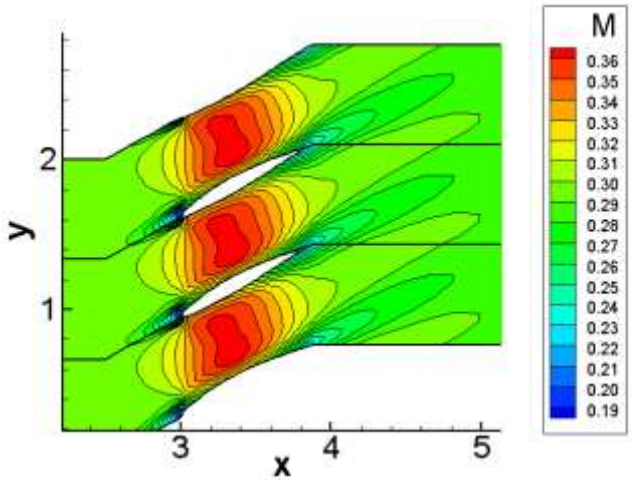

Figure 5 Mach number distribution in case of initial geometry

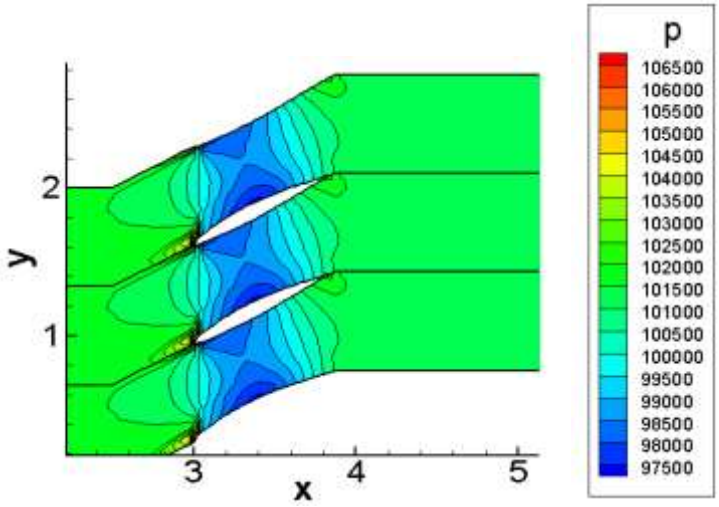

Figure 6 Static pressure distribution in case of initial geometry

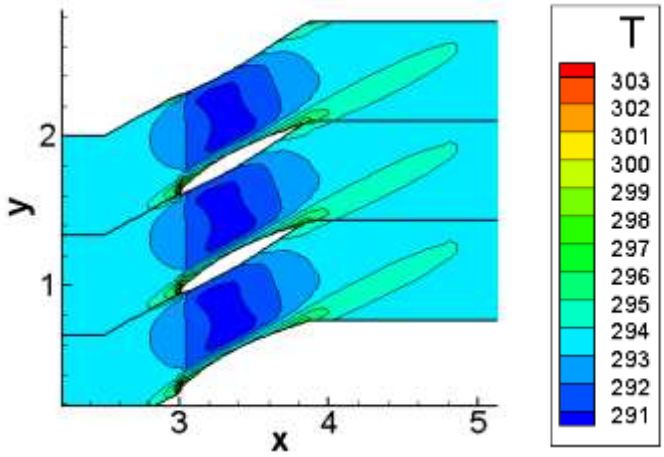

Figure 7 Static temperature distribution in case of initial geometry

Application of the Optimization Procedure

NACA 65-410 profile has been used also for testing the correct operation of the inverse design solver. The boundary conditions are the followings: inlet total pressure: $p_{tot,in}$=107853.4 [Pa]; inlet total temperature: $T_{tot,in}$=298.4 [K]; inlet flow angle: 30° and the outlet static pressure: $p_{stat,out}$=101325 [Pa] over the H-type mesh (110×60).

The optimum pressure distribution belongs to the maximum area of the closed distribution of the suction side is generated by the SQP method at the limit of separation in case of adverse pressure gradient flow conditions on the suction side. However, several points near to the leading edge of the suction side are modified to make the extremely high pressure gradient smoother (see Fig. 8). Moreover, an arbitrary (optimal) target pressure distribution often causes non-realistic geometry as negative thickness, trailing edge opening or cross over. Based on several theoretical investigation and computational tests, it can be noticed, that the expected pressure distribution cannot be arbitrary in case of subsonic flow due to the information propagation into the upstream (leading edge) direction along the streamline bounded by the wall. If the required pressure is differ from the initial one at the certain representative part of the near wall region, the flow can be retarded or sucked depends on the local conditions. This effect has an influence on the flow evolution starting from the leading edge and the pressure should be redistributed by considering higher or lower local kinetic energy along the stream line especially at the first couple mesh points of the leading edge [17].

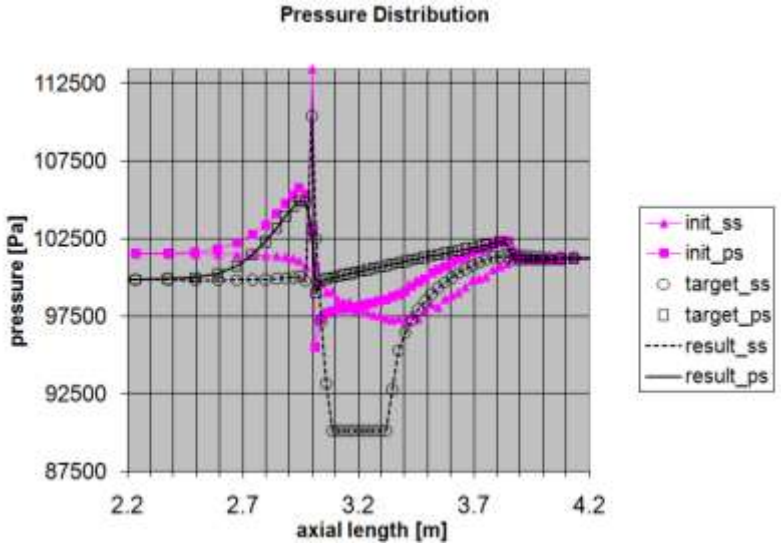

Figure 8 Comparison of the initial, target and result static pressure distributions over the suction and pressure side of the profile (ss: suction side, ps: pressure side)

So, the modified distributions are imposed in the inverse design procedure to determine the geometry, which provides the expected conditions. The inverse design method was converged after 10 iteration cycles of the inverse, wall modification and direct modes. The normal velocity distribution across the solid wall is near to zero at the 10th iteration of the inverse subroutine, which represents that there is no need for further steps, the pressure gradient is infinitesimally small (no flow) across the solid boundary. The corresponding results of the optimization procedure are found in Fig. 8. The target and optimised (result) pressure distribution are compared with each other and the deviation between them is negligible. The inverse design method with Stratford's separation prediction theory based SQP nonlinear constrained optimization method can be used as an optimization tool after further investigation and deeper research. The optimized, redesigned geometry with Mach number, pressure and temperature distribution are found in Fig. 9-11.

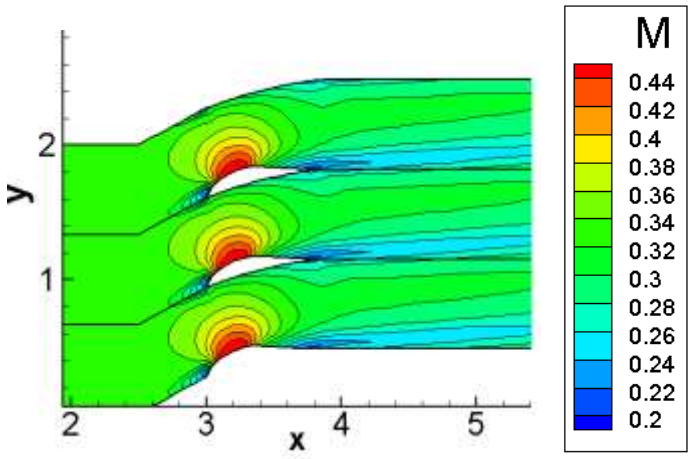

Figure 9 Mach number distribution in case of redesigned geometry

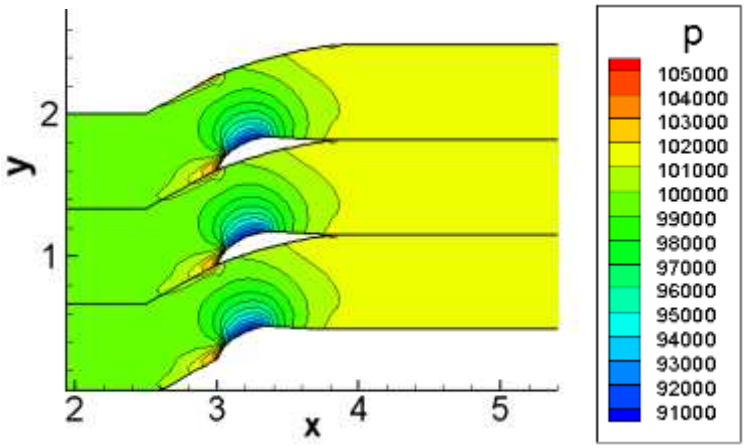

Figure 10 Static pressure distribution in case of redesigned geometry

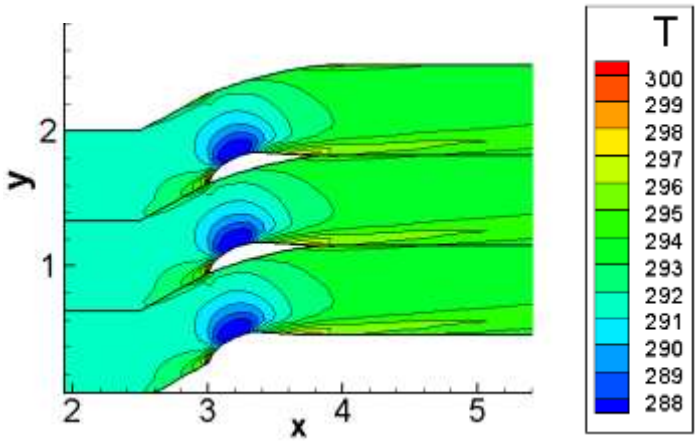

Figure 11 Static temperature distribution in case of redesigned geometry

VERIFICATION OF THE RESULTS BY MEANS OF ANSYS CFX

ANSYS CFX has been used for the analyses of the optimized, redesigned blade in order to compare the result of DASFLOW and ANSYS CFX with each other at the same mesh, boundary conditions, material properties and physical settings. The simulations in ANSYS CFX have been performed by two different approaches: inviscid and viscous flow regime to see the difference between them and the (inviscid) in-house code.

Inviscid Analysis of the Optimized and Redesigned Blade by CFX

The first step is the model generation. The Design Modeller, which is part of ANSYS Workbench, has been used for creating the flow field. The 2D coordinates of the points are imported from the Tecplot_21_10.dat file into the Design Modeller. Lines and 3D splines have been created by using the read points in order to define the contours of the domain. 3 periodic pairs, inlet and outlet together with the suction and pressure side of the profile form the 2D boundaries of the blade

channel to be modelled. The flow domain is created by extruding this surface by three cell size-distances defined afterwards and valid between the suction and pressure side of the blade. Concerning the numerical mesh, similar configuration has been created in the present case also than in DASFLOW model to minimize the differences between the two computational approaches. Before transferring the model in the mesh generation module and defining the element size for the spatial discretisation, all the lines and surfaces are suppressed. For each part of the cascade, the size, number of division and bias factors has been defined in the mesher submodule. Choosing the "Number of Divisions" and entering a value in the "Number of Divisions" field is an alternative way to define "Element Size" if one is interested in having the mesh to be sized according to a discrete number of divisions along an edge. The properties of the meshes are shown in Table 1 for horizontal direction. For the vertical edges (4 edges) the numbers of divisions were 13 and no bias factor has been defined. The so-called "Hex Dominant Method" is used for the meshes, which means that the domain is filled with hexahedron elements. In order to create a structural mesh the "Mapped Face Meshing" option has been used. The created mesh is found in Fig. 12.

Horizontal edges (4 edges)	Number of divisions	Bias factor
Surface 1	9	5
Surface 2	10	3.67
Surface 3	33	1
Surface 4	19	18.5

Table 1 Discretization for the mesh generation. The number of nodes was 3522 and the number of elements was 2362

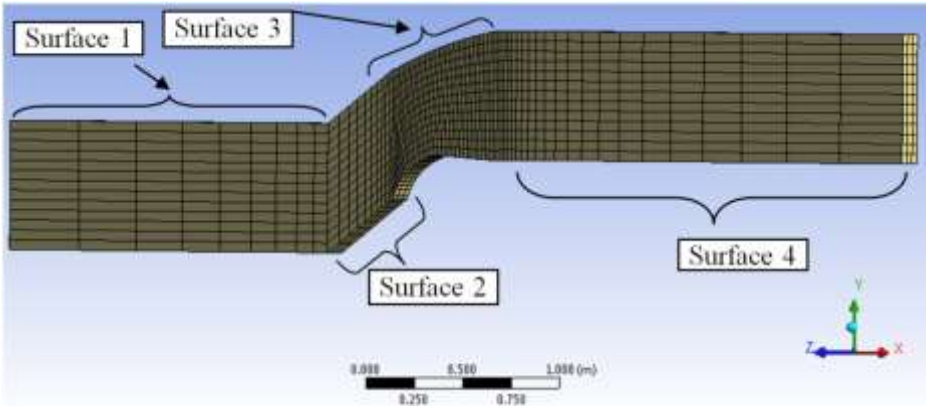

Figure 12 General mesh configuration of the fluid region for inviscid case – ANSYS CFX

In CFX-Pre sub module, the properties of the operational fluid through the domain have been defined. Air as an ideal gas with zero viscosity is used. The reference pressure has been set up to be 100000 Pa. The option of heat transfer corresponds to 'Total Energy'. Free slip boundary condition has been used for solid surfaces. The boundary conditions are the following: inlet total pressure: $p_{tot,in}$=107853.4 [Pa]; inlet total temperature: $T_{tot,in}$=298.4 [K]; inlet flow angle: 30° and the outlet static pressure: $p_{stat,out}$=101325 [Pa]. After reaching the convergence criterion, the results

of the CFX are evaluated. First, the pressure distributions, as quantitative results, are shown in the upstream, downstream periodic pairs and over the suction and pressure side of the profile (see Fig. 13). The initial, the target and the result pressure distributions of DASFLOW are also presented beside the inviscid result of CFX for the pressure side (Ansys-ps) and the suction side (Ansys-ss).

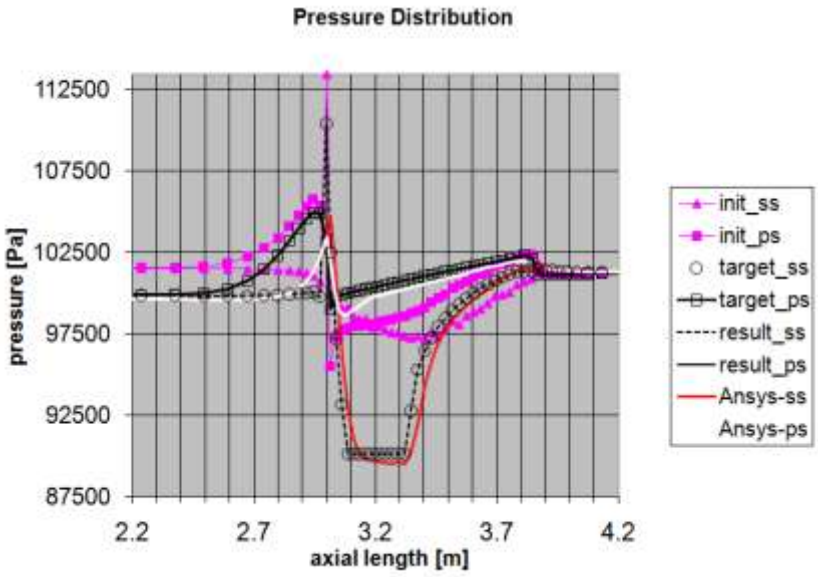

Figure 13 Pressure distribution of the redesigned blade configuration in case of inviscid analysis of DASFLOW and ANSYS (ss=suction side, ps=pressure side)

The difference between the two approaches is less than 5 % percent, which is acceptable. The one of the main difference is at the leading edge stagnation point. The static pressure in DASFLOW is much higher compared with CFX. This unphysical feature is caused by the linear extrapolation of determining static pressure at the ghost cell of the solid wall boundaries. This pressure is plotted in the diagram in case of DASFLOW without completing averaging procedure.

The qualitative results are also available in case of CFX for comparison. The Mach number distribution is plotted in FIG. 14. The Mach number reaches the maximum value of 0.52 compared with DASFLOW, which has a value of 0.45 in that region (see Fig. 9). Concerning the maximum static pressure provided by DASFLOW, it is 105500 [Pa] (see Fig. 10) and it is 105000 in case of CFX (see Fig. 15). The differences in both cases are mostly due to the different treatment of the boundary conditions and its averaging over the cells. However, the used discretization methods can also contribute to have different results based on the different inherent mechanism.

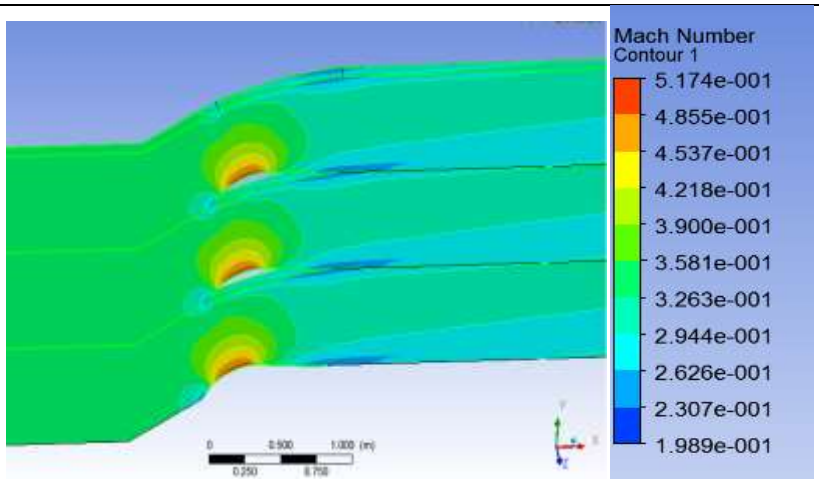

Figure 14 Mach number distribution of the redesigned blade configuration in case of ANSYSCFX (inviscid analysis)

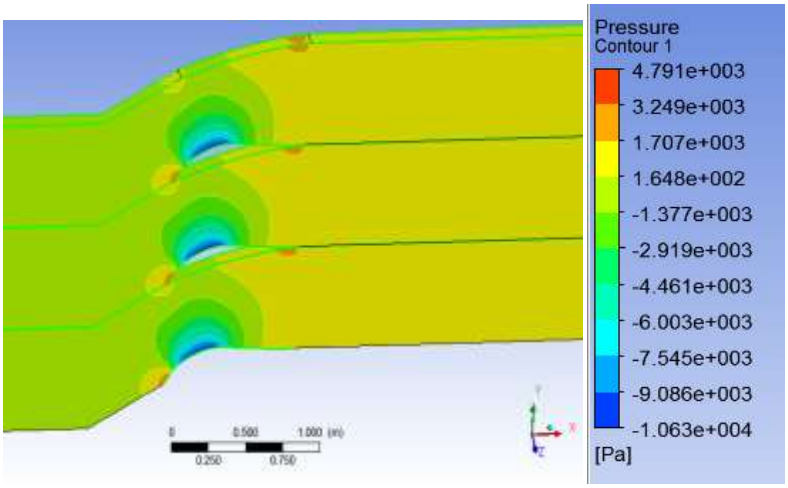

Figure 15 Pressure distribution of the redesigned blade configuration in case of ANSYSCFX (inviscid analysis)

Viscous Analysis of the Optimized and Redesigned Blade by CFX

Although the same procedure has been followed in viscous analysis also than in case of the inviscid analysis, there are some differences between the two approaches. The boundary layer is resolved on such a way that the first cell from the wall to be fallen in the log layer region. Hence, dimensionless analytical expressions are used to determine the distance of the first cell from the wall to have y+=21.

Air is considered as an ideal gas for operational fluid with the reference pressure of 100000 Pa. The value of the dynamic viscosity has been set to be 1.831e-05 Pas. Total energy has been used for the heat transfer. Shear stress transport (SST) turbulence model has been applied.

The boundary conditions are the following: inlet total pressure: $p_{tot,in}$=107853.4 [Pa]; inlet total temperature: $T_{tot,in}$=298.42 [K]; inlet flow angle: 30° and the outlet static pressure: $p_{stat,out}$=101325 [Pa]. No slip boundary condition is used for wall boundary condition.

After having convergent results, first, the quantitative results are shown in Fig. 16. The initial, the target and the result pressure distributions of DASFLOW are also presented beside the inviscid (Ansys-ss and Ansys-ps) and viscous (Ansys-ss-viscous and Ansys-ps-viscous) result of the CFX software (ss=suction side and ps=pressure side). The difference between the two approaches is less than 5 %, which is acceptable. The one of the main difference is at the leading edge stagnation point also. The static pressure in DASFLOW is higher compared with CFX due to the same reason as it is mentioned in the subchapter 5.1.

The qualitative results are also investigated in case of CFX for comparison. The relative static pressure distribution is plotted in FIG. 17. The relative static pressure reaches the maximum value of 105700 compared with DASFLOW, which has a value of 105500 in that region (see Fig. 10). The difference is negligible.

Both, the viscous and inviscid analyses provide accurate modelling for the presented flow regime, which is acceptable in engineering point of view. Hence, the presented inverse design based optimization method - after sensitivity analyse, further plausibility check - can be used in design and developments in the field of the fluid dynamics.

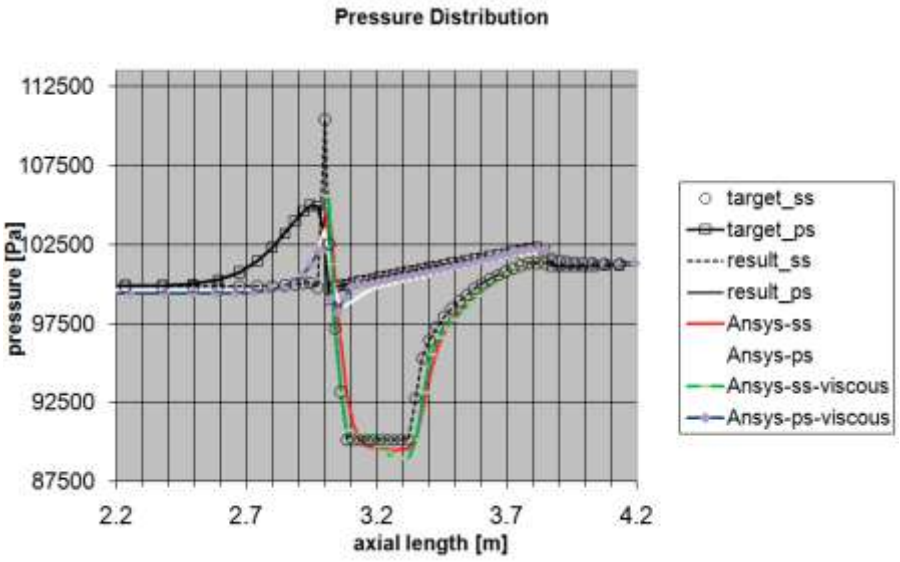

Figure 16 Pressure distribution of the redesigned blade configuration in case of inviscid analysis of DASFLOW and inviscid and viscous analysis of ANSYS (ss=suction side, ps=pressure side)

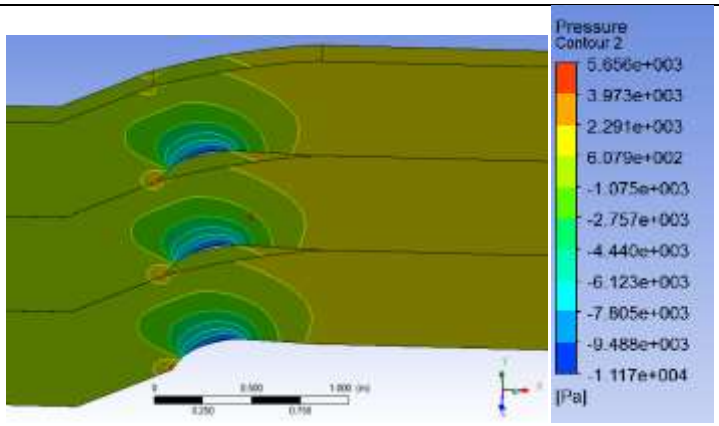

Figure 17 Pressure distribution of the redesigned blade configuration in case of ANSYS CFX (viscous analysis)

CONCLUSIONS

Numerical investigations were completed in the present research in order to verify the correct operation and the accuracy of the DASFLOW inverse design based optimization tool. The used academic code has been implemented in object oriented C++ environment and it has been developed at Budapest University of Technology and Economics, Department of Aeronautics, Naval Architecture and Railway Vehicles.

Concerning the flow solver, the convective fluxes of the Euler equations are discretized by Roe's approximated Riemann method with MUSCL approach and Mulder limiter. The number and determination of the physical and numerical boundary conditions are based on the theory of characteristics.

A conventional inverse design method is coupled with a nonlinear SQP constraint optimization algorithm and has been used to determine the geometry belongs to the highest blade loading at given operational conditions. The goal function of the optimization is the maximum area of the closed surface bounded by the suction side pressure distributions in the function of chord length. Stratford's limiting flow theory is used to evaluate pressure in each points of the suction side providing maximum flow deceleration close, but safe distance far from the separation.

A specific modification of the optimum pressure distribution is used near to the leading edge before executing inverse design subroutine to avoid unrealistic solutions as trailing edge opening or cross over. The modification allows the designer to suck out or push back the first part of the profile artificially, which can have a favourable effect on curing the cross over or opening problems.

The optimization method is tested successfully over the cascade created by NACA 65-410 profile at certain operational conditions defined by the inlet total pressure, inlet total temperature, inlet flow angle and outlet static pressure conditions to determine the corresponding profile belongs to the required pressure distribution developed by the non-linear constrained optimization by considering Stratford's flow limiting theory. The results are realistic. ANSYS CFX commercial

code has been used for plausibility check. Viscous and inviscid type flow analysis shows that the average deviation is less than 5 percent between the results of DASFLOW and ANSYS. Hence, the presented inverse design based optimization method – after sensitivity analyse, further plausibility check – can be used in design and developments in the field of the fluid dynamics.

REFERENCES

[1] HAYNI CLABUK - VIJAY MODI Optimum Plane Diffusers In Laminar Flow, J. Fluid Mechanics, 237, 373-393, 1992.

[2] A. DEMEULENAERE An Euler/Navier-Stokes Inverse Method for Compressor and Turbine Blade Design, Von Kármán Institute for Fluid Dynamics, Inverse Design and Optimisation Methods, Lecture Series (1997-05), 1-45, 1997.

[3] LAURENT DE VITO - RENE VAN DEN BRAEMBUSSCHE - HERMAN DECONINCK A Novel Two-dimensional Viscous Inverse Design Method for Turbomachinery Blading, International Gas Turbine and Aeroengine Congress and Exhibition, Amsterdam, PAYS-BAS (03/06/2002), vol. 125, n2, pp. 310-316, 2003.

[4] MICHAEL B. GILES - MARK DRELA Two-Dimensional Transonic Aerodynamic Design Method, AIAA, Journal 25(9), 1199-1206, 1987.

[5] CHARLES HIRSCH Numerical Computation of Internal and External Flows, Vol. II, Computational Methods for Inviscid and Viscous Flows, John Wiley & Sons, Chichester, 1990.

[6] DMITRI KUZMIN - MATTHIAS MÖLLER Algebraic Flux Correction II. Compressible Euler Equations, http://www.mathematik.tu-dortmund.de/papers/KuzminMoeller2004a.pdf, (07.03.2015) 1990.

[7] CULBERT B. LANEY Computational Gas dynamics, Cambridge University Press, 1998.

[8] M. LEFEBVRE - T. ARTS Numerical Aero-thermal Prediction of Laminar/Turbulent Flows in a Two-dimensional High Pressure Turbine Linear Cascade, Second European Conference on Turbomachinery - Fluid Dynamics and Thermodynamics, Antwerp, Belgium, pp. 401-409, 1997.

[9] M. J. LIGHTHILL A Method of Two-dimensional Aerodynamic Design, R&M 2112, Aeronautical Research Council, London, 1945.

[10] MARCHELLO MANNA A Three Dimensional High Resolution Compressible Flow Solver, PhD thesis, Catholic University of Leuven, 1992.

[11] P. L. ROE Approximate Riemann Solvers, Parameter Vectors, and Difference Schemes, Journal of Computational Physics, Vol. 43 pp. 357-372, 1981.

[12] A. M. O. SMITH High-Lift Aerodynamics, Journal of Aircraft, Vol. 12 No. 6, pp. 501-530, 1975.

[13] E. STEIN - R. BORST - T. HUGHES Finite volume methods, foundation and analysis, Edited by John Wiley & Sons, Ltd. c 2004.

[14] B. S. STRATFORD The Prediction of Separation of the Turbulent Boundary Layer, Journal of Fluid Mechanics, Vol. 5. pp 1-16, 1959.

[15] DOMINIQUE THÉVENIN - GÁBOR JANIGA Optimization and Computational Fluid Dynamics, Hardcover, ISBN 978-3-540-72152-9, Springer-Verlag Berlin Heidelberg, 2008.

[16] H. C. YEE A class of high-resolution explicit and implicit shock-capturing methods, VKI lecture series 1989-04, March 6-10, 1989, NASA TM-101088, Feb. 1989.

[17] ÁRPÁD VERESS - ATTILA FELFÖLDI – TAMÁS GAUSZ –LÁSZLÓ PALKOVICS: Coupled Problem of the Inverse Design and Constraint Optimization, Applied Mathematics and Computation 219:(13) pp. 7115-7126. Paper AMC 16476, 2013.

[18] ÁRPÁD VERESS - TIBOR GALLINA -JÓZSEF ROHÁCS Fast and Robust Inverse Design Method for Internal and Cascade Flows, International Review of Aerospace Engineering (IREASE), ISSN 1973-7459 Vol. 3 N. 1. pp. 41-50. February, 2010.

[19] KÁROLY BENEDA CFD Simulation of Blade Load Distribution Control as Active Centrifugal Compressor Surge Suppression, ACTA AVIONICA 15:(25) pp. 13-20, 2013.

[20] KÁROLY BENEDA Numerical Simulation of MEMS-based Blade Load Distribution Control in Centrifugal Compressor Surge Suppression, ICNPAA 2012 Congress, Mathematical Problems in Engineering, Aerospace

and Sciences, Vienna, Austria, 10.07.2012.-14.07.2012, AIP Conference Proceedings, Volume 1493. Issue 1, pp. 116-123, 2012.

[21] ANDRÁS NAGY - JÓZSEF ROHÁCS - TAMÁS RÉGERT Investigation on the Effect of Hydrodynamic MEMS on Airfoil, 26th International Congress of the Aeronautical Sciences (ICAS), Anchorage, USA, 14.09.2008.-19.09.2008, Edinburgh: Optimage Ltd., pp. 1-10. PAPER ICAS2008-3.10. ISBN: 0-9533991-9-2, 2008.